Ocean Engineering 195 (2020) 106674

Contents lists available at ScienceDirect

Ocean Engineering

journal homepage: www.elsevier.com/locate/oceaneng

Flume tank evaluation of the hydrodynamic lift and drag of helix ropes compared to conventional ropes used in midwater trawls

Gebremeskel Eshetu Kebede [a,*], Paul D. Winger [a], Harold DeLouche [a], George Legge [a], Zhaohai Cheng [a], David Kelly [b], Haraldur Einarsson [c]

[a] Centre for Sustainable Aquatic Resources, Fisheries and Marine Institute, Memorial University, 155 Ridge Rd., St. John's, Newfoundland and Labrador, A1C 5R3, Canada
[b] Hampidjan Canada Ltd., 527 Conception Bay Hwy, Spaniard's Bay, Newfoundland and Labrador, A0A 3X0, Canada
[c] Marine and Freshwater Research Institute, Skúlagata 4, 101 Reykjavík, Iceland

ARTICLE INFO

Keywords:
Helix
Drag
Lift
Drag coefficient
Lift coefficient
Attack angle
Reynolds number

ABSTRACT

The hydrodynamic properties of ropes can significantly affect the underwater performance of midwater trawls, including their geometry, drag, fuel consumption, and rate of gear setting and hauling activities. In this study, we investigate the hydrodynamic properties of helix ropes compared to conventional polyethylene (PE) and nylon (PA) ropes. Flume tank tests were conducted using 17 different braided and twisted ropes of varying diameter (6 mm, 8 mm, 9 mm, and 14 mm). Samples of each rope type were subjected to a series of water velocities (0.5 m/s, 0.7 m/s, and 0.9 m/s) and angles of attack (0°, 12°, 20°, 45°, 61°, and 90°) in order to measure drag and lift forces. To understand how hydrodynamic coefficients vary with increasing Reynolds number (Re), we also evaluated a wider range of water velocities (0.3 m/s to 0.9 m/s) for 14 mm ropes. Our results showed that, when compared to conventional ropes of the same diameter, helix ropes produced increased lift force (*L*), verifying their description as self-spreading ropes. To our knowledge, these findings represent the first known evidence of its kind published in scientific literature with direct application to midwater trawling operations.

1. Introduction

Ropes are a dominant structural component of midwater trawls used for commercial fishing. They vary widely in their size, shape, and design and are found throughout the entire fishing system, including warps, sweeps, bridles, headline, fishingline, and forward panels of the trawl (Garner, 1978; Sainsbury, 1996). The resulting underwater shape of a trawl and the 3-dimensional (3D) position of various trawl components are greatly affected by the hydrodynamic properties of the ropes used in its construction. Thus, studies on the interaction between ropes and fluids can be helpful to fishing gear designers, in particular the importance of the geometry and orientation of strands in a rope and how they affect the lift and drag forces in towing applications, such as midwater trawls.

Helical ropes, commonly known as helix ropes, are similar in many respects to traditional ropes, but include the added feature of a smaller rope twisted over the surface of the main rope. The physical shape is very similar to a cylinder with thinner wire twisted over the surface. Thus, previous scientific findings on cylinders with an outer helical wire can be instructive for current and future studies on helix ropes used in fishing gears. There are a number of past studies on fluid patterns around plain, rough, and helical-covered cylindrical structures. By disrupting fluid flow around a cylinder by using rough elements or helical fins on the surface, a reduction in structural vibration and stress can be obtained, as well as enhancing the early transition of the laminar boundary layer into turbulent flow, resulting in a smaller drag coefficient (Rhahi, 1991; Yang et al., 1994). Evidence has shown that the addition of roughness on the surface of a cylinder can shift the boundary layer at transition state to a lower Reynolds number ($\approx 8 \times 10^4$) compared to the transition state of a smooth cylinder at Reynold number ($\approx 2 \times 10^5$) (Achenbach, 1971; Potter et al., 2016). Moreover, adding rough structures on the surface may shift the separation point closer to the rear stagnation point, resulting in a smaller wake width and less drag (Rhahi, 1991). For instance, the attachment of a triangular wedge pointing downstream on the rear side of a smooth cylinder can reduce the drag coefficient from 1.19 to 0.89 (Hoerner, 1965). For

* Corresponding author. Fisheries and Marine Institute of Memorial University, Centre for Sustainable Aquatic Resources, 155 Ridge Rd., St. John's, Newfoundland and Labrador, A1C 5R3, Canada.
E-mail address: gebre.kebede@mi.mun.ca (G.E. Kebede).

https://doi.org/10.1016/j.oceaneng.2019.106674
Received 1 November 2018; Received in revised form 5 September 2019; Accepted 2 November 2019
Available online 9 November 2019

wire-wrapped cylinders below the subcritical regime, when the wire diameter is appreciably less than the size of the boundary layer thickness, there is no change in drag coefficient with respect to corresponding values of smooth cylinders. However, when the helical wire diameter is much larger than the estimated boundary layer thickness, the drag coefficient becomes greater than the corresponding value for a smooth cylinder (Nassif et al., 1989). Winkel and Paschen (2005) documented the transverse force that is produced when these types of structures are placed in a flow field.

An Icelandic gear technologist named Hjörtur Erlendsson first invented helix rope for midwater trawling in 1997. The ropes are composed of three components, including a core or inner product, over braided sheath, and an outer helical rope as shown in Fig. 1. Use of this product in the forward sections of a midwater trawl to enhance mouth opening (referred to as self-spreading trawls) was soon developed and patented (Safwat and Perevoshchikov, 2005; Erlendsson and Safwat, 2012). Since that time, self-spreading trawls have been successfully introduced to the global market (Hampidjan, 2018). However, little if any scientific literature has been published on the effectiveness of helix ropes and their potential benefits to midwater trawling. This has motivated us to answer how the physical size, orientation, and material-composition affect the hydrodynamic performance.

The objective of this study was to investigate the hydrodynamic performance of helix ropes in comparison to conventional polyethylene (PE) and nylon (PA) ropes of the same diameter. We conducted a series of flume tank tests using helix ropes as well as braided or twisted PE and PA ropes of different lays and thicknesses. We measured the hydrodynamic drag and lift forces under various test conditions and calculated the associated hydrodynamic coefficients. The results are compared across the different types of ropes with a discussion on the application to midwater trawling.

2. Materials and methods

2.1. Materials

In this experiment, seventeen different types of ropes were evaluated (Table 1). Samples were purchased from Hampidjan AS, Reykjavik, Iceland. Six of the ropes were helix ropes with varying diameters and helical rope configurations (Fig. 1). The core is hydrophilic, denser than water, accounting for 47% by mass. The over braided sheath is composed of polyethylene (PE), contributing 30% by mass. The outer helical rope is also composed of PE, contributing 23% by mass. The remaining eleven ropes were conventional PE and PA twisted or braided ropes with different diameters (Table 1). Each rope was given a code to identify its physical specifications. For example, HES-6 stands for Helix, S-lay, with 6 mm diameter. For helix ropes, letters 'd' and 'D' indicate the diameter of the helical and core ropes respectively, and 'P' indicates the pitch of the helical rope, which is the distance between the loops.

A metal frame was constructed from round stock aluminum (diameter 12.7 mm) for supporting the ropes in the flume tank (Fig. 2) in the manner similar to Lee et al. (2007) and Madsen et al. (2011). Its dimensions were 1.524 m × 1.524 m (L x W). Each rope type was sequentially mounted and tested using the frame. For 6 mm ropes, we mounted 18 rope strands of the same rope type on the frame spaced at 7.5 cm between each strand. For 8 mm, 9 mm, and 14 mm ropes, we mounted 8 rope strands of the same rope type on the frame spaced at 14 mm between each strand.

Hydrodynamic evaluations were conducted using the flume tank located at the Fisheries and Marine Institute, Memorial University, Newfoundland and Labrador, Canada (see Winger et al., 2006 for specifications). Dimensions of the test chamber are 22.5 m × 8 m x 4 m (L x W x D). Maximum water velocity is 1.0 m/s.

2.2. Test setup

2.2.1. Measurement of lift and drag forces

We applied a general crossflow principle for the measurement of drag and lift forces as it has been shown to work well in uniform water flow in subcritical flows ($Re < 1 \times 10^5$) (see Garrison, 1985; Hoerner, 1965; Norton et al., 1981). Lift and drag forces generated by the frame were measured in the manner similar to the evaluation of otter boards (Seafish, 1995). See Fig. 3a for an illustration of how the frame was arranged in the flume tank. We used two types of load cells: 22.7 Kg load cell (Model-LFS 270-UV, Cooper Instruments & Systems, USA) and 45.4 Kg load cell (Model-No. 31, Honeywell, USA). One of the load cells was positioned parallel to the direction of the water flow for the purpose of measuring drag (D), while the other was positioned perpendicular to water flow for the purpose of measuring lift (L). Yaw rotation along the Z-axis was performed by shortening a pair of bridles on the port side of

Fig. 1. Sample of 14 mm helix ropes of S-lay in left side and Z-lay on the right side.

Table 1
List of ropes used in this study, including material, interlacing pattern, total projected area (*S*), and diameter (*D*). For helix ropes, d indicates the diameter of the helical ropes and P indicates the pitch of the helical rope.

Sample	Rope type	Material	Interlacing Pattern	Code	Number of ropes per sample	S (m^2)	D (mm)	P (mm)	d (mm)
1	Helix	Composite	S-lay	HES-6	18	2.69E-01	6	17	4
2	Helix	Composite	S-Lay	HES-8	8	1.40E-01	8	27	5
3	Helix	Composite	S-lay	HES-14	8	2.17E-01	14	32	9
4	Helix	Composite	Z-Lay	HEZ-6	18	2.36E-01	6	17	4
5	Helix	Composite	Z-Lay	HEZ-8	8	1.38E-01	8	27	5
6	Helix	Composite	Z-Lay	HEZ-14	8	2.14E-01	14	32	9
7	Braided	PA	–	PA-6	18	1.94E-01	6	–	–
8	Braided	PA	–	PA-8	8	1.18E-01	8	–	–
9	Braided	PA	–	PA-14	8	2.09E-01	14	–	–
10	Twisted	PA	S-lay	PAS-9	8	1.68E-01	9	–	–
11	Twisted	PA	S-lay	PAS-14	8	1.69E-01	14	–	–
12	Twisted	PA	Z-lay	PAZ-9	8	1.32E-01	9	–	–
13	Twisted	PA	Z-lay	PAZ-14	8	1.29E-01	14	–	–
14	Braided	PE	–	PE-6	18	1.95E-01	6	–	–
15	Twisted	PE	Z-lay	PEZ-6	18	1.18E-01	6	–	–
16	Twisted	PE	Z-lay	PEZ-8	8	1.95E-01	8	–	–
17	Twisted	PE	Z-lay	PEZ-14	8	1.94E-01	14	–	–

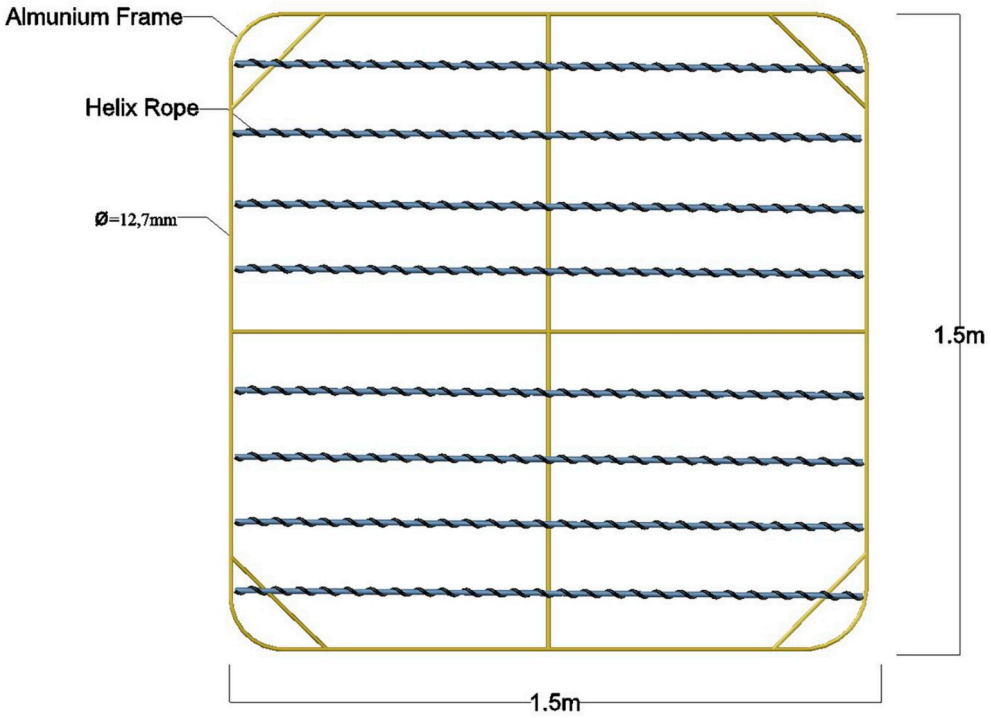

Fig. 2. Line drawing of the aluminum metal frame with rope strands stretched horizontally across the frame.

the frame in order to produce mean angles of attack of 0°, 12°, 20°, 45°, 61°, and 90°. The angle of attack of the frame for each rope and test condition was determined using an overhead camera filming top down in horizontal XY plane and analyzing the resulting images using Image J software. The corresponding bridle lengths were: 0.00 m, 0.87 m, 1.08 m, 1.69 m, 1.89 m and 2.02 m, respectively. The length of pair of bridles on the starboard side were 2.02 m each. For each test condition, the metal frame with rope samples was subjected to water velocities of 0.5 m/s, 0.7 m/s, and 0.9 m/s.

2.3. Calculation of hydrodynamic coefficients

Measurement of the drag and lift forces was based on Newton's first law, sometimes called the first law of equilibrium. For each test condition, the hydrodynamic resistance force on the frame was resolved into two components: drag (*D*) and lift (*L*) forces (Fridman and Carrothers, 1986). The corresponding coefficients of the drag and lift force were determined by:

$$C_d = \frac{2D}{\rho S V^2} \tag{1}$$

$$C_l = \frac{2\mathrm{L}}{\rho S V^2} \tag{2}$$

where C_d and C_l are the drag and lift coefficients, D and L are the measured drag and lift forces respectively (kgf), ρ is density of the water ($9.996 \times 10^2\,\mathrm{kgm}^{-3}$), V is water velocity (m/s), and S is the total projected area (m^2) of the rope strands. Estimates of projected area of the ropes on the frame were determined by image analysis of photographs for each test condition using Image J software.

In order to investigate the relationship between hydrodynamic coefficients and increasing Reynolds number (Re), each of the 14 mm

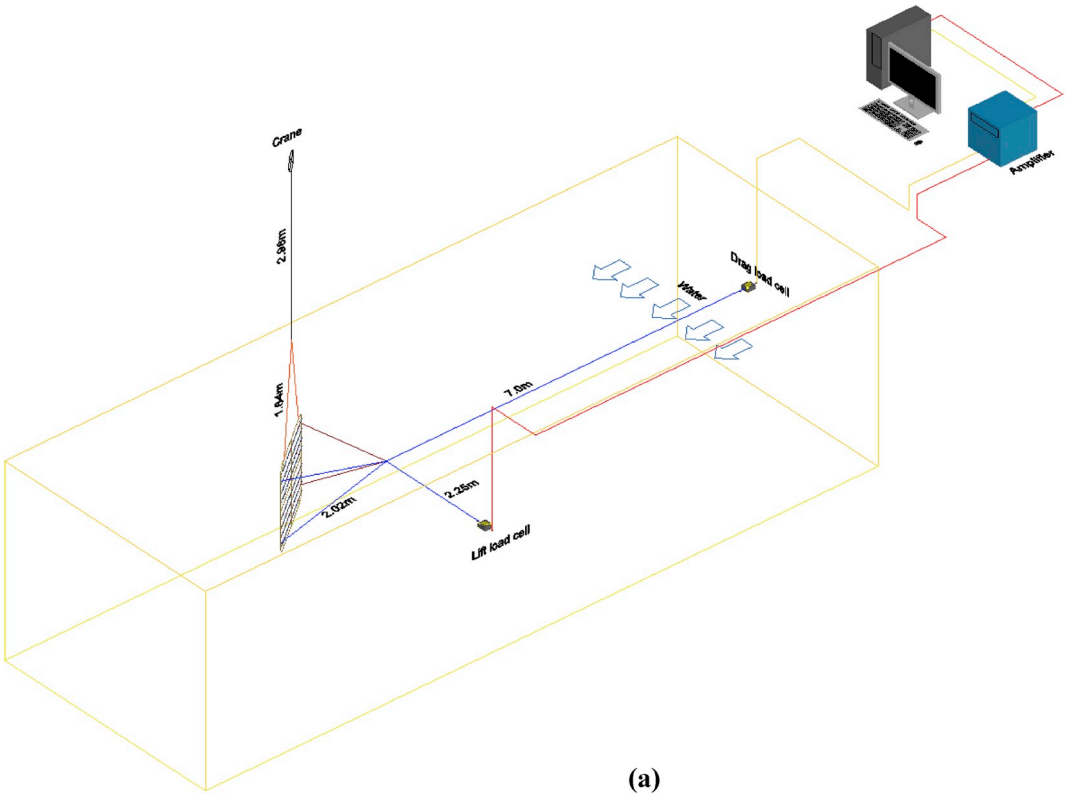

(a)

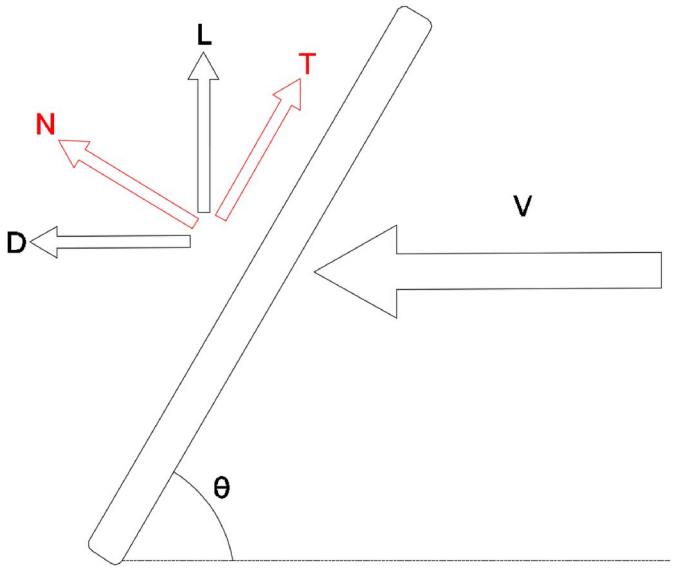

(b)

Fig. 3. (a) Schematic drawing of the experimental setup in the flume tank, (b) Components of resistance force resolved into Drag (D), and Lift (L), and resistance force is resolved into normal (N) and tangential (T) force components.

ropes were also subjected to water velocities ranging from 0.3 to 0.9 m/s at 0.1 m/s intervals at a single angle of attack (20°). Our goal was to mimic the orientation of rope bars used in the meshes of wing panels of midwater trawls. Reynolds number (Re) was expressed as:

$$Re = \frac{VD}{\nu} \tag{3}$$

where V is the water velocity (m/s), D is the diameter of ropes (m) measured using Vernier calipers at 20 equally spaced locations along the rope samples, and ν is the kinematic viscosity of water at 10 °C ($1.33 \times 10^{-6} m^2 s^{-1}$).

Past research has shown that the drag and lift forces of nets vary as a function of net solidity, Reynolds number, and angle of attack to water

flow (Bi et al., 2014; Hosseini et al., 2011; Lader and Enerhaug, 2005). Of all the models proposed, the cross-flow principle developed by Hoerner (1965) is the best fitting model for predicting hydrodynamic coefficients (Madsen et al., 2011). Here, we modified the form of the equation suggested by Hoerner (1965) by considering frictional coefficients that we determined at Re = 0 (i.e. at no flow condition), the coefficients of drag (C_d (θ)) and lift (C_l (θ)) as function of attack angle are expressed as:

$$C_d(\theta) = (C_{d90} - C_{d0})\ sin^3\theta + C_{d0} \quad (4)$$

$$C_l(\theta) = (C_{d90} - C_{d0})\ sin^2\theta\ cos\theta + C_{l0} \quad (5)$$

where C_{d90} and C_{d0} are the calculated coefficient of drag at 90° and 0° attack angles, and C_{l0} is the calculated lift coefficient at 0° attack angle.

2.4. Normal and tangential resistance forces

The hydrodynamic force on a rope is represented only in the plane defined by water speed and the rope which is sum of lift and drag forces. Lift (L) is the sum of vertical forces due to components pressures and shears, and Drag (D) is the sum of the horizontal forces due to components pressures and shears (Cengel, 2010; Garrison, 1985; Hoerner, 1965). This is put into a more general form referred to as the cross-flow principle; where L is normal to the flow and D is inline with the flow, both of which are components of the resistance force (R) which is normal to the rope when rope aligned at a certain angle to flow direction. However, the resultant resistance force direction is dependent on drag and lift forces (Fridman and Carrothers, 1986; Hoerner, 1965) (see Fig. 3b). Moreover, when the rope is parallel to the water flow, the resistance force will be in the same direction as of flow and drag. The magnitude of the resistance force (R) is expressed as:

$$R = \left(L^2 + D^2\right)^{1/2} \quad (6)$$

The resistance force also can also be defined as) the sum of normal force (N) and tangential force (T), and its magnitude expressed as:

$$R = \left(N^2 + T^2\right)^{1/2} \quad (7)$$

However, the tangential and resistance forces are related by an equation;

$$T = \frac{N}{tan\theta} \quad (8)$$

where θ is the angle of attack. In a similar manner, the coefficient of resistance force (C_R) can be obtained from drag and lift coefficients. The coefficient of tangential force (C_T) can be determined from the angle of attack and normal force coefficient (C_N).

2.5. Data treatment and statistical analysis

Millivolt signals generated by the load cells were processed using a signal-conditioning amplifier which boosted the signal to a level (0–10 VDC) compatible with our data acquisition hardware which logged the data at a frequency of 50 Hz. The resulting loads (kgf) were imported into MS Excel for initial data exploration and removal of outliers (see Tsukrov et al. (2011) for methodology). The known force of the bare frame (without ropes) for each test condition was then subtracted to determine the forces generated by the ropes themselves. The processed dataset was saved as text-tab delimited file for statistical analysis using R-studio software.

For comparison of the drag and lift coefficients, we used the two-sample Kolmogorov Smirnov test to compare each of the datasets collected at each water velocity and angle of attack. We used one-way ANOVA and Tukey HSD (Tukey honest significant difference) to compare the mean lift and drag forces produced by the ropes.

3. Results

3.1. Coefficients of lift and drag

Fig. 4a–c illustrates the relationship between the coefficient of lift (C_l) and angle of attack for conventional and helix ropes at varying water velocities. In general, the maximum C_l was obtained at 45° and 61° for all rope types, while the minimum C_l was obtained at 0° and 90° angles of attack. Variation among the rope types was most notable at the 61° angle of attack. For example, at a water velocity of 0.9 m/s and an angle of attack of 61°, the C_l for HES-6, HEZ-6, and PA-6 were 0.62, 0.66, and 0.47 respectively. For 8 mm ropes under the same conditions, the C_l for HES-8, HEZ-8, and PA-8 were 0.55, 0.59 and 0.54 respectively. Similarly, for 14 mm ropes, the C_l of HES-14, HEZ-14, and PA-14 were 0.55, 0.57 and 0.57 respectively. However, despite few variation in C_l values, most pairwise comparisons revealed no significant differences among the coefficients for a given rope diameter, water velocity, and angle of attack (i.e. D value < D critical at α = 0.25). In other words, neither the direction of lay (S or Z), material (PA or PE), or the presence/absence of the helix helical had a detectable effect on the resulting coefficient of lift (C_l) ($p > 0.05$).

Fig. 5a–c illustrates the relationship between the coefficient of drag (C_d) and the angle of attack for conventional and helix ropes at varying water velocities. For all rope types, the lowest C_d occurred at 0°, increasing rapidly with increasing angle of attack. Deviation in C_d among the different rope types was most notable at the 61° and 90° angles of attack. For example, at a water velocity of 0.9 m/s and an angle of attack of 90°, the C_d for HES-6, HEZ-6, and PA-6 were 1.91, 1.99, and 1.79 respectively. For 8 mm ropes under the same conditions, the C_d for HES-8, HEZ-8, and PA-8 were 1.81, 1.72 and 1.71 respectively. Similarly, for 14 mm ropes, the C_d for HES-14, HEZ-14, and PA-14 were 1.81, 1.8 and 1.72 respectively. However, despite few variation in C_d values, most pairwise comparisons revealed no significant differences among the coefficients for a given rope diameter, water velocity, and angle of attack (D-value < D-critical, α = 0.25). In other words, neither the direction of lay (S or Z), material (PA or PE), nor the presence/absence of the helix had a detectable effect on the resulting coefficient of drag (C_d) ($p > 0.05$).

Fig. 6 illustrates the drag and lift coefficients of 6 mm rope samples calculated using the cross-flow principle described in Equations (4) and (5). Both conventional and helix ropes show a very similar trend with increasing angle of attack. The relationship for C_d was sigmoidal, characterized by an increasing slope near 30°, maximum steepness near 60°, decreasing slope near 80°, with maximum C_d values observed at 90°. The relationship for C_l was bell shaped, characterized by minimum values at 0° and 90° and maximum values near 55°. The trend was also very similar to that obtained by Madsen et al. (2011) and Kristiansen et al. (2015) for different fiber net panels.

3.2. Lift and drag forces

Figs. 7 and 8 provide a direct comparison of the lift and drag (kgf) forces observed for the different rope types at a water velocity of 0.9 m/s and 20° angle of attack, which are the conditions most comparable to trawling applications. The results reveal that, for a given rope diameter, the type of rope had significant effect on both the lift and drag measured (see Table 2ā b for ANOVA results). These differences were statistically detectable for both lift and drag at all three diameters ($p < 0.001$). For 6 mm ropes, the mean lift force for HES-6, HEZ-6 and PA-6 was 2.24 kg, 2.49 kg, and 2.08 kg respectively. Similarly, for 8 mm ropes, HES-8 and HEZ-8 showed 9.32% and 9.74% increase with respect to PA-8. Once again, for 14 mm ropes, HES-14 and HEZ-14 gained 7.9% increase and 8.6% increase with respect to PA-14.

For 6 mm ropes, drag force for HES-6, HEZ-6 and PA-6 were 5.51 kg,

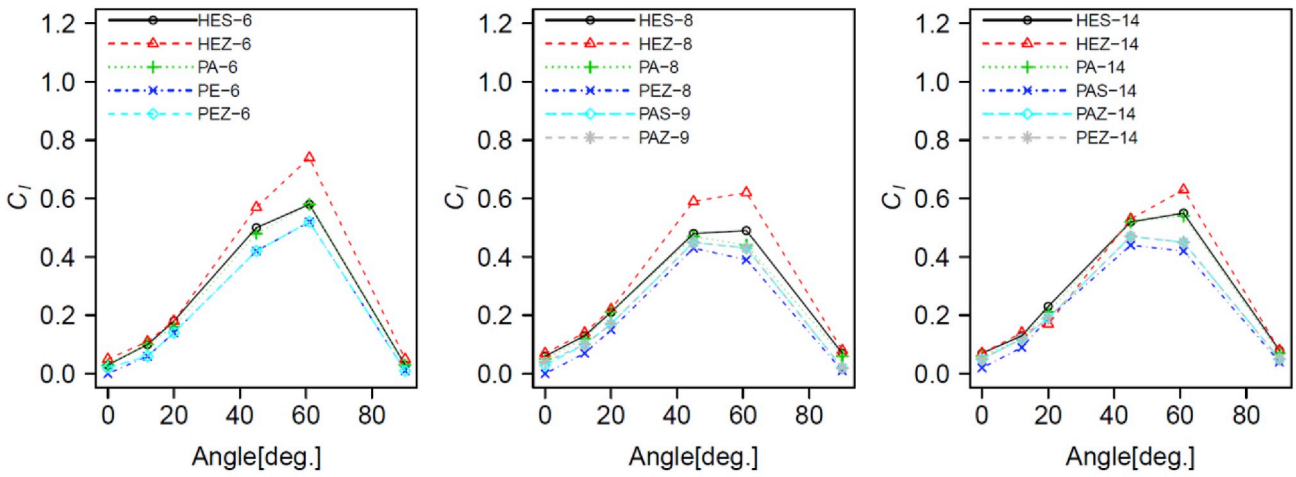

(a) At 0.5m/s

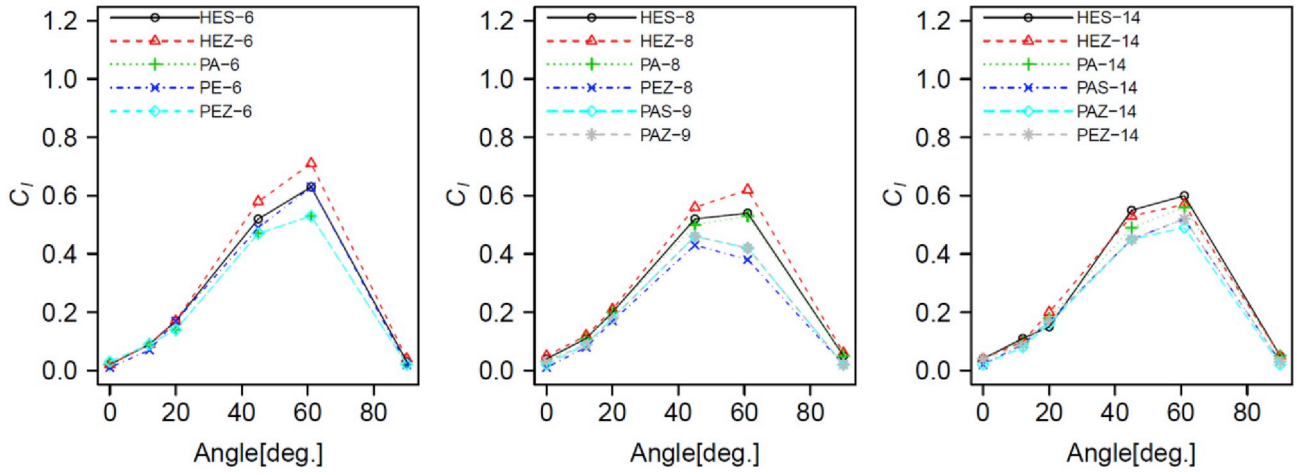

(b) At 0.7 m/s

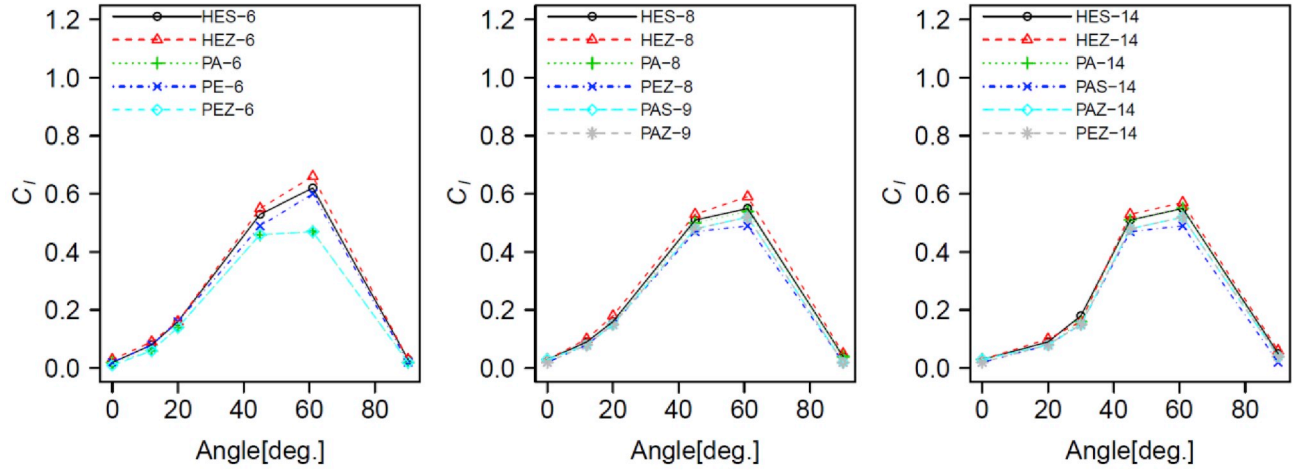

(c) At 0.9m/s

Fig. 4. Relationship between coefficient of lift (*Cl*) and angle of attack for the different rope types at 0.5 m/s, 0.7 m/s, and 0.9 m/s water velocities.

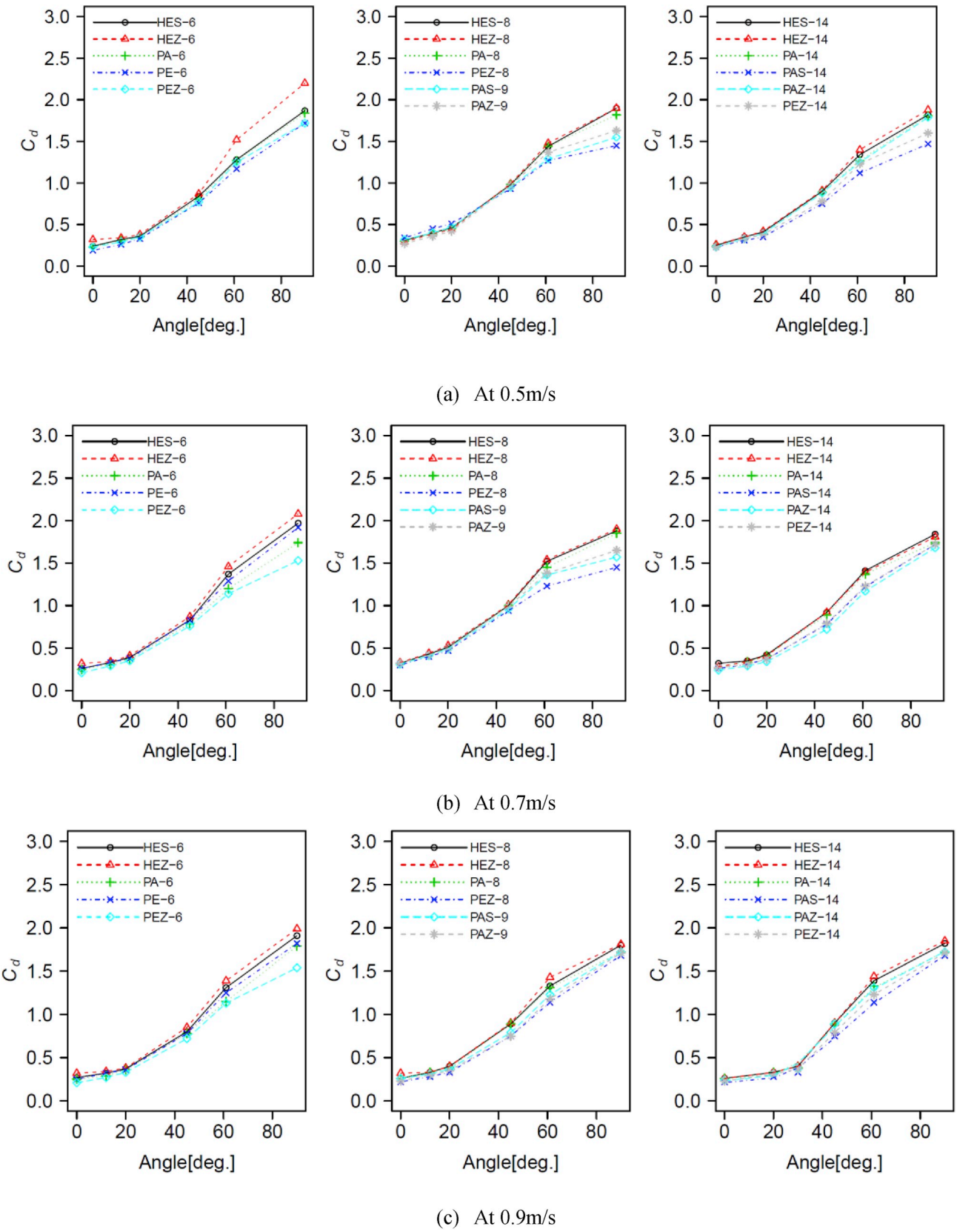

Fig. 5. Relationship between the coefficients of drag (*Cd*) and angle of attack for the different rope types at 0.5 m/s, 0.7 m/s, and 0.9 m/s water velocities.

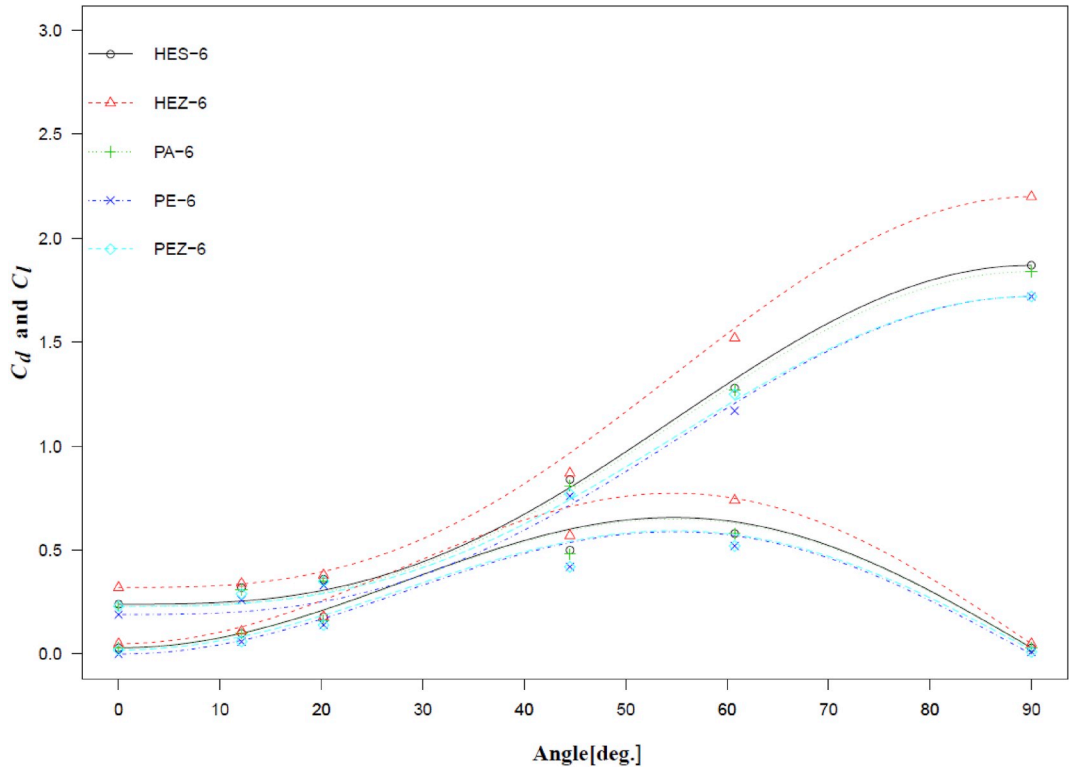

Fig. 6. Modeling of the drag and lift coefficient using crossflow principle for 6 mm at 0.5 m/s.

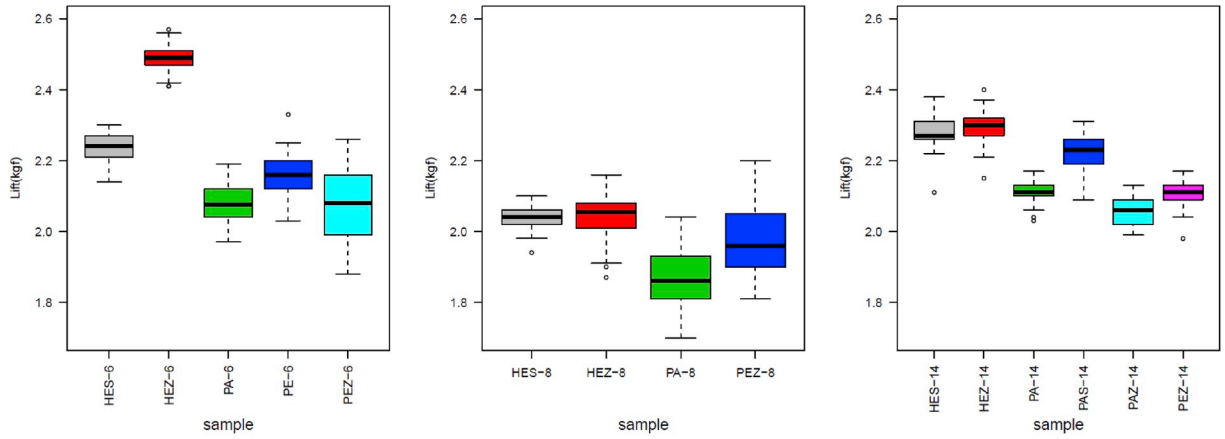

Fig. 7. Box plots of the lift forces observed for 6 mm, 8 mm, and 14 mm ropes at 20° attack angle at 0.9 m/s water velocity.

5.58 kg, and 4.85 kg respectively. Similarly, for 8 mm rope samples, HES-8, and HEZ-8 possessed 6.9% and 9.3% increase with respect to PA-8. For 14 mm rope samples, HES-14, and HEZ-14 gained a 19.5% and 15.5% increase with respect to PA-14. Subsequent pairwise comparisons are shown in Fig. 9.

3.3. Effect of Reynolds number

Hydrodynamic coefficients of ropes in trawling applications depends on their geometry, material composition, and Reynolds number (Fridman and Carrothers, 1986). Using data collected in the previous experiment, we examined the hydrodynamic coefficients (C_l and C_d) with increasing Reynolds number (Re) for the 14 mm ropes (HES-14, HEZ-14, and PA-14). Fig. 10 reveals inconsistency at lower Reynolds numbers; however, for Reynolds numbers above 8×10^3, the mean deviations of C_l of the HES-14 and HEZ-14 with respect to PA-14 were 31.3% and 18.8%. For C_d, both conventional and helix ropes showed very similar values for Re ranges from 4×10^3 to 10×10^3, however for Re above 10×10^3, the mean deviations of C_d of the HES-14 and HEZ-14 with respect to PA-14 were 5.1% and 7.7%. Kolmogorov Smirnov pairwise comparisons revealed no statistical difference (D-value < D-critical, $\alpha = 0.05$) for any corresponding pair of C_l and C_d at each water velocity.

3.4. Coefficients of normal and tangential resistance forces

Normal (C_N) and tangential (C_T) force coefficients were calculated for 14 mm rope samples, specifically: HES-14, HEZ-14, and PA-14. Table 3 lists the resulting values at different angles of attack and a water velocity of 0.9 m/s. Overall, the coefficient of tangential force (C_T) showed a declining trend with increasing attack angle, however the coefficient of normal force (C_N) showed an increasing trend with

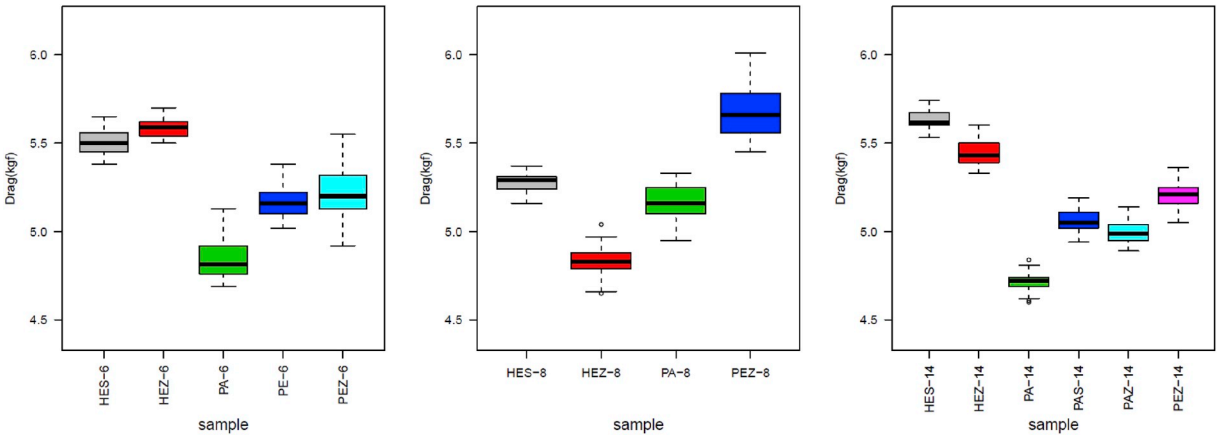

Fig. 8. Box plots of the drag forces observed for 6 mm, 8 mm, and 14 mm ropes at 20° attack angle at 0.9 m/s water velocity.

Table 2a
Analysis of variance (ANOVA) of the mean lift forces observed at 20° attack angle.

Category	Parameters	DF	Sum of squares	Mean squares	F value	p-value
6 mm ropes	Sample	4	5.84	1.46	393.2	<2e-16***
	Residuals	245	0.91	0.0037		
8 mm ropes	Sample	3	1.052	0.3506	66.02	<2e-16***
	Residuals	196	1.041	0.0053		
14mmropes	Sample	5	2.491	0.4983	310.3	<2e-16***
	Residuals	294	0.472	0.0016		

Significance code (α): 0 '***'.

Table 2b
Analysis of variance (ANOVA) of the mean drag forces observed at 20° attack angle.

Category	Parameters	DF	Sum of squares	Mean squares	F value	p-value
6 mm ropes	Sample	4	17.292	4.323	436	<2e-16***
	Residuals	245	2.429	0.010		
8 mm ropes	Sample	3	18.178	6.059	651.9	<2e-16***
	Residuals	196	1.822	0.009		
14 mm ropes	Sample	5	27.037	5.407	1468	<2e-16***
	Residuals	294	1.083	0.004		

Significance code (α): 0 '***'.

increasing attack angle as it is mainly dependent on the drag coefficient. Moreover, tangential force coefficients in conventional and helix ropes are shown to be very similar at different attack angles.

4. Discussion

Previous studies evaluating the hydrodynamic forces produced by ropes and netting have been conducted at flume tanks located in South Korea (Lee et al., 2007) and Denmark (Madsen et al., 2011). Our study was similar to these experiments in its use of a metal frame rotated in the yaw direction to achieve different angles of attack to the water current. However, our experimental design differed with respect to instrumentation. Lee et al. (2007) and Madsen et al. (2011) both mounted their metal frame directly to a multi-axis force/torque sensor for the measurement of lift and drag forces. Our design by comparison, used two-inline load cells for the measurement of drag and lift forces. Our yaw rotation was controlled by shortening a pair of bridles, which was time consuming, and proved difficult for attaining a desired attack angle. Nevertheless, our approach was found to perform well, producing accurate and repeatable estimates of lift and drag.

Lift forces were higher for helix ropes compared to conventional ropes when tested at the same water velocities and angles of attack. This represents the first known evidence of its kind published in the scientific literature. It supports the claims of existing patents (e.g., Safwat and Perevoshchikov, 2005; Erlendsson and Safwat, 2012) and validates the concept of self-spreading midwater trawls (Hampidjan, 2018). Though not directly investigated in this study, the ability of helix ropes to increase lift has significant application for midwater trawling. Use of helix ropes could theoretically increase the mouth opening of a trawl, allowing vessels to achieve the same mouth opening as conventional trawls, but with reduced door size, floatation on the headline, and weights on the footline. This in turn, could reduce fuel consumption, gear size, speed up hauling and setting operation, and improve fishing efficiency.

Drag forces were higher for helix ropes compared to conventional ropes when tested at the same water velocities and angles of attack. We attribute this finding to the fact that our flume tank could only achieve a maximum velocity of 0.9 m/s. Thus we conducted our experiment within the subcritical region (low Re) (Nassif et al., 1989) and were not able to observe an earlier transition and a quick declining trend of drag for the helical ropes. We speculate that a reduction in drag would have been detected had we tested at higher velocities (i.e., higher Re). Achenbach (1971) found that the surface roughness of the cylinder had no effect on drag at low Reynold numbers in subcritical regions. However, at upper end of subcritical, the early transition of the laminar boundary to turbulent boundary can be obtained through the addition of a helical wire on a smooth cylinder (Yang et al., 1994). This transition might be attained at Re between 2×10^4–10×10^4 (Potter et al., 2016). Goldstein (1938) found at Re above 5.0×10^4, drag reduction could be attained by placing thinner wires at $\pm 65°$ from front stagnation point around a smooth cylinder. This arrangement was able to delay the separation by causing the boundary layer to become turbulent which resulted in reduced drag. In another study, Ferro (1990) documented that stranded (rough) cables had lower drag coefficient than smooth cables when towed behind a research vessel at velocities between 0.4 m/s ~2.8 m/s. Taken together, these results lead us to speculate that at higher water velocities, the helix ropes used in this study would exhibit reduced drag in comparison to conventional ropes. Moreover, trend of the hydrodynamic coefficients at low Reynolds numbers (<0.3 m/s flow speed) should be investigated in the future.

5. Conclusion

In this study, we observed the basic parameters that are essential for characterizing the hydrodynamic properties of ropes (helix, nylon, and polyethylene) used for construction of midwater trawls. Using a flume tank, we evaluated the drag and lift forces for 17 different ropes at

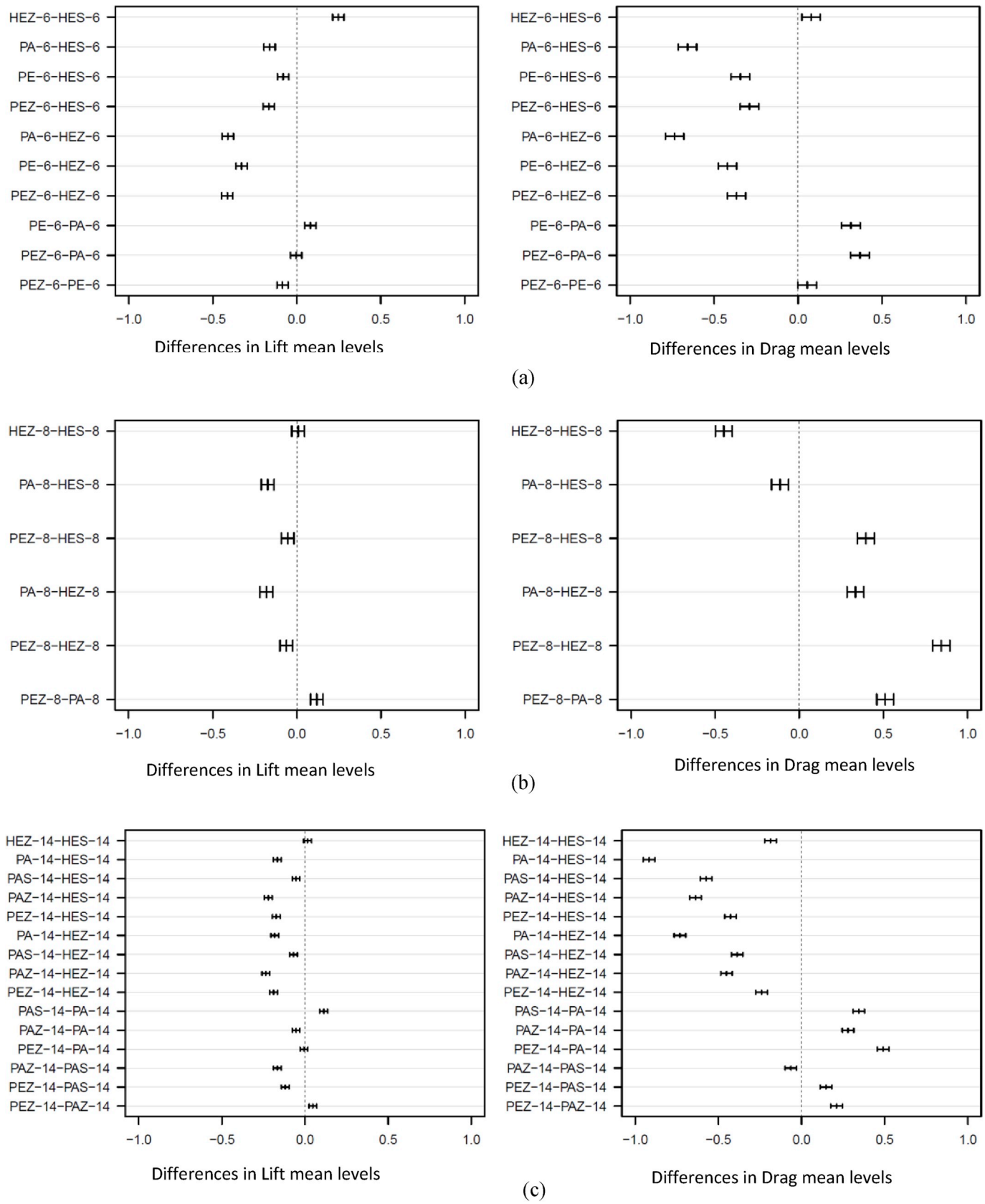

Fig. 9. Tukey HSD plot for comparison of the means of lift and drag forces of 6 mm (a), 8 mm (b), and 14 mm (c) rope samples at 20° attack angle and 0.9 m/s water velocity.

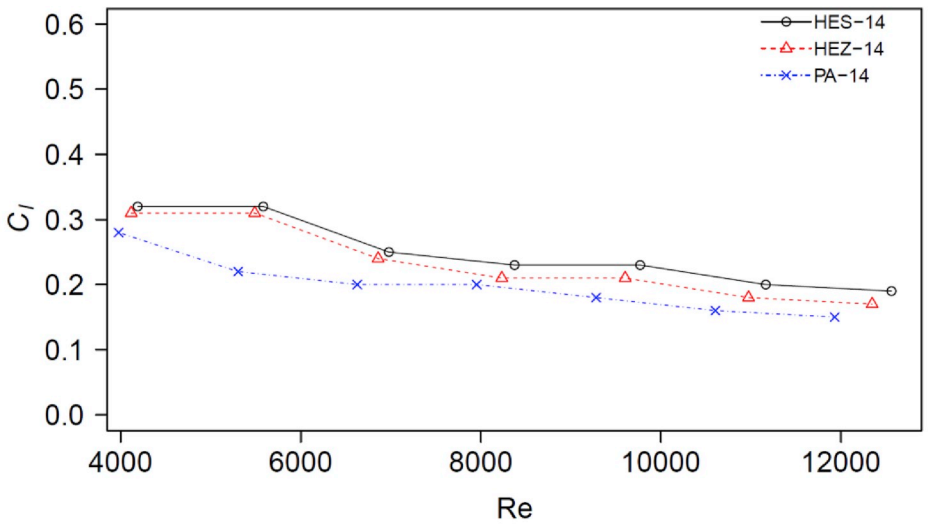

(a)

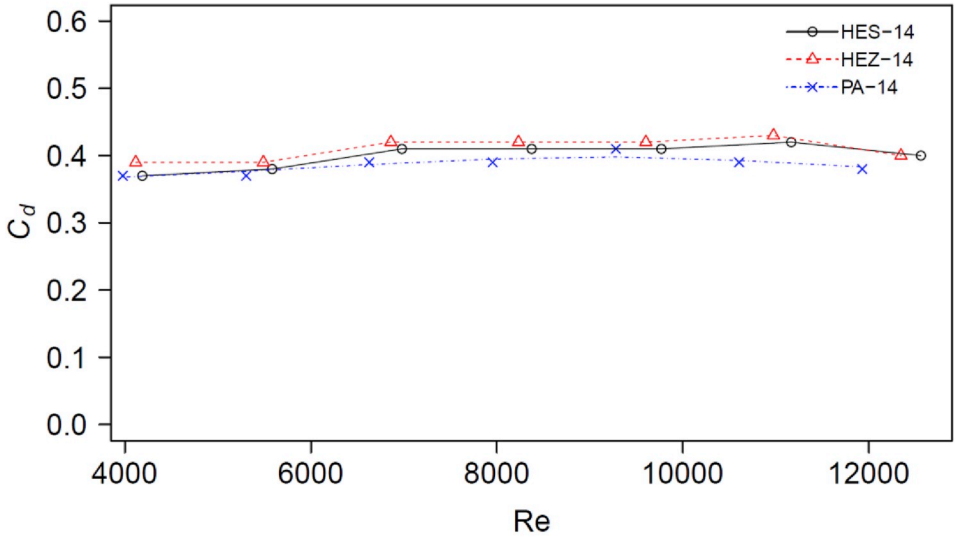

(b)

Fig. 10. Hydrodynamic coefficients (*Cl* and *Cd*) for 14 mm rope samples with Reynolds number at 20° attack angle.

Table 3
Normal and Tangential force coefficients for 14 mm ropes.

Attack Angle (°)	Helix Slay 14 mm (HES-14)		Helix Zlay 14 mm (HEZ-14)		PA14mm (HES-14)	
	C_N	C_T	C_N	C_T	C_N	C_T
0°	0.32	–	0.26	–	0.3	–
12°	0.34	1.62	0.31	1.47	0.3	1.6
20°	0.42	1.16	0.38	1.06	0.4	1.2
45°	1.04	1.04	0.91	0.91	1.0	1.0
61°	1.44	0.80	1.30	0.72	1.5	0.8
90°	1.81	0.00	1.80	0.00	1.7	0.0

various water velocities and angles of attack. In summary, we found these results based on comparative analysis in specified test conditions [$4.51 \times 10^2 < \mathrm{Re} < 1.24 \times 10^4$];

- No statistical difference was detected among coefficients of lift (C_l) and drag (C_d) for helix and conventional ropes.
- Lift (L) forces were higher for helix ropes compared to conventional ropes.
- Drag (D) forces were higher for helix ropes compared to conventional ropes.

In conclusion, the hydrodynamic properties of helix ropes are uniquely different from conventional polyethylene (PE) and nylon (PA) ropes. However, the study was not without its limitations. Due to the slower water velocities used (≤0.9 m/s), we did not detect a reduction in drag for helix ropes, which was expected. We recommend future studies be conducted at higher velocities (higher Re) as well as numerical simulation using computational Fluid dynamics (CFD), both of which can more closely approximate actual towing speeds [2.8–4.0kn] of midwater trawls.

Acknowledgements

This study was funded by the Ocean Frontier Institute (OFI), Canada; Fisheries and Marine Institute of Memorial University, Canada. Special thanks to Craig Hollett and Ryan Doody for calibration of load cells and

for assisting with flume tank testing as well as Michael Pol, Stephen Walsh, and Carl Harris for their scientific and engineering advice.

References

Achenbach, E., 1971. Influence of surface roughness on the cross-flow around a circular cylinder. J. Fluid Mech. 46 (2), 321–335.

Bi, C.W., Zhao, Y.P., Dong, G.H., Zheng, Y.N., Gui, F.K., 2014. A numerical analysis on the hydrodynamic characteristics of net cages using coupled fluid–structure interaction model. Aquacult. Eng. 59, 1–12.

Cengel, Y.A., 2010. Fluid Mechanics. McGraw-Hill, p. 983p.

Erlendsson, H., Safwat, S., 2012. Lower drag helix rope for pelagic trawls and methods. Google Patents. https://patents.google.com/patent/US20120118131. (Accessed 28 September 2018).

Ferro, R.S.T., 1990. Force Coefficients for Stranded and Smooth Cables. Scottish Fisheries Research Report No. 47. Department of Agriculture and Fisheries for Scotland, 10p.

Fridman, A.L., Carrothers, P., 1986. Calculations for Fishing Gear Designs. Fishing News Books, England, p. 241p.

Garner, J., 1978. Pelagic and Semi-pelagic Trawling Gear. Fishing News Books Ltd., Farnham, p. 59p.

Garrison, C.J., 1985. Comments on cross-flow principle and Morison's equation. J. Waterw. Port, Coast. Ocean Eng. 111 (6), 1075–1079.

Goldstein, S. (Ed.), 1938. Modern Developments in Fluid Dynamics: an Account of Theory and Experiment Relating to Boundary Layers, Turbulent Motion and Wakes, vol. 1. Clarendon Press, p. 310p.

Hampidjan, 2018. Gloria self-spreading pelagic trawls. http://www.hampidjan.is/products/fishing/trawls/pelagic-trawls/. (Accessed 28 September 2018).

Hoerner, S.F., 1965. Fluid-dynamic drag: practical information on aerodynamic drag and hydrodynamic resistance. Midland Park, N.J. 455p.

Hosseini, S.A., Lee, C.W., Kim, H.S., Lee, J., Lee, G.H., 2011. The sinking performance of the tuna purse seine gear with large-meshed panels using numerical method. Fish. Sci. 77 (4), 503–520.

Kristiansen, D., Fore, M., Aarsæther, K.G., Fredheim, A., 2015. Numerical Simulation of Complex Systems Involving Interaction between Elements with Large and Varying Stiffness. https://brage.bibsys.no/xmlui/bitstream/handle/11250/2451070/A27066-+FinalReport_NumSim-David+Kristiansen.pdf?sequence=2. Accessed March 2019.

Lader, P.F., Enerhaug, B., 2005. Experimental investigation of forces and geometry of a net cage in uniform flow. IEEE J. Ocean. Eng. 30 (1), 79–84.

Lee, M.K., Lee, C.W., Song, D.H., 2007. Experiments on hydrodynamic coefficients of netting in relation to mesh grouping. Proceedings: Methods for the Development and Evaluation of Maritime Technologies, DEMaT, pp. 35–44, 2007.

Madsen, N., Hansen, K., Enerhaug, B., 2011. Experimental analysis of the hydrodynamics cofficients of net panels in the flume tank in Hirtshals. In: Proceedings: Methods for the Development and Evaluation of Maritime Technologies, DEMaT, 2011, pp. 131–140.

Nassif, M.Y., Tom, S., Rahi, H.R., Nakayama, A., 1989. Flow over Wire-Wrapped Cylinders at Low Reynolds Number, vol. 34. Bulletin of the American Physical Society. America, Mechanical Engineering Report.

Norton, D.J., Heideman, J.C., Mallard, W.W., 1981. January. Wind tunnel tests of inclined circular cylinders. In: Offshore Technology Conference. Offshore Technology Conference.

Potter, M.C., Wiggert, D.C., Ramadan, B.H., 2016. Mechanics of fluids. Nelson Educ. 793p.

Rhahi, L.H.A., 1991. Turbulent wakes of wire wrapped cylinders. Forum on Turbulent Flows 112, 95–100.

Safwat, S., Perevoshchikov, V., 2005. Self-spreading trawls having a high aspect ratio mouth opening. Google Patents. https://patents.google.com/patent/US20050160656A1. (Accessed 28 September 2018).

Sainsbury, J.C., 1996. Commercial Fishing Methods: an Introduction to Vessels and Gears, third ed. Fishing News Books Ltd., Oxford, p. 359p.

Seafish, 1995. Otterboard performance and behaviour. Commission of the European communities FAR. Contract (1), 214p.

Tsukrov, I., Drach, A., DeCew, J., Swift, M.R., Celikkol, B., 2011. Characterization of geometry and normal drag coefficients of copper nets. Ocean Eng. 38 (17–18), 1979–1988.

Winger, P.D., DeLouche, H., Legge, G., 2006. Designing and testing new fishing gears: the value of a flume tank. Mar. Technol. Soc. J. 40, 44–49.

Winkel, H.J., Paschen, M., 2005. January. Hydrodynamic loads on twisted ropes and hawsers. In: ASME 2005 24th International Conference on Offshore Mechanics and Arctic Engineering. American Society of Mechanical Engineers, pp. 775–785.

Yang, E.E., Rahai, H.R., Nakayama, A., 1994. Mean pressure distribution and drag coefficient of wire-wrapped cylinders. ASME J. Fluid. Eng. 116 (2), 376–378.